

RI 9490

RI 9490

REPORT OF INVESTIGATIONS/1994

PLEASE DO NOT REMOVE FROM LIBRARY

LIBRARY
SPOKANE RESEARCH CENTER
RECEIVED

FEB 10 1994

US BUREAU OF MINES
E. 315 MONTGOMERY AVE.
SPOKANE, WA 99207

Erosive Wear of Potential Valve Materials for Coal-Conversion Plants

By L. Garner McDonald and John E. Kelley

UNITED STATES DEPARTMENT OF THE INTERIOR



BUREAU OF MINES

U.S. Department of the Interior
Mission Statement

As the Nation's principal conservation agency, the Department of the Interior has responsibility for most of our nationally-owned public lands and natural resources. This includes fostering sound use of our land and water resources; protecting our fish, wildlife, and biological diversity; preserving the environmental and cultural values of our national parks and historical places; and providing for the enjoyment of life through outdoor recreation. The Department assesses our energy and mineral resources and works to ensure that their development is in the best interests of all our people by encouraging stewardship and citizen participation in their care. The Department also has a major responsibility for American Indian reservation communities and for people who live in island territories under U.S. administration.

Report of Investigations 9490

Erosive Wear of Potential Valve Materials for Coal-Conversion Plants

By L. Garner McDonald and John E. Kelley

UNITED STATES DEPARTMENT OF THE INTERIOR
Bruce Babbitt, Secretary

BUREAU OF MINES

International Standard Serial Number
ISSN 1066-5552

CONTENTS

	<i>Page</i>
Abstract	1
Introduction	2
Acknowledgments	4
Curve-fit equations for three-dimensional plots	4
Test equipment	6
Materials	6
Procedures	6
Results and discussion	7
Particle impingement angle effects	7
Particle velocity effects	11
Summary	11
References	12
Appendix A.—Comments on materials	13
Appendix B.—Test data	14

ILLUSTRATIONS

1. Lockhopper ball-valve and valve-seat damaged by entrained particle erosion	2
2. Let-down valve liner damaged by entrained particle erosion	3
3. Erosion test equipment	6
4. Effect of velocity and impingement angle on specific wear of 316 stainless steel eroded by 27- μm alumina	8
5. Effect of velocity and impingement angle on specific wear of annealed 440-C stainless steel eroded by 27- μm alumina	8
6. Effect of velocity and impingement angle on specific wear of hardened 440-C stainless steel eroded by 27- μm alumina	8
7. Effect of velocity and impingement angle on specific wear of HC-250 white cast iron eroded by 27- μm alumina	8
8. Effect of velocity and impingement angle on specific wear of Haynes 6B cobalt-based superalloy eroded by 27- μm alumina	9
9. Effect of velocity and impingement angle on specific wear of K-68 cobalt-bonded tungsten carbide eroded by 27- μm alumina	9
10. Effect of velocity and impingement angle on specific wear of 316 stainless steel eroded by 50- μm alumina	9
11. Effect of velocity and impingement angle on specific wear of annealed 440-C stainless steel eroded by 50- μm alumina	9
12. Effect of velocity and impingement angle on specific wear of HC-250 white cast iron eroded by 50- μm alumina	10
13. Effect of velocity and impingement angle on specific wear of Haynes 6B cobalt-based superalloy eroded by 50- μm alumina	10
14. Effect of velocity and impingement angle on specific wear of K-701 cobalt and chromium-bonded tungsten carbide eroded by 50- μm alumina	10
15. Effect of velocity and impingement angle on specific wear of K-801 nickel-bonded tungsten carbide eroded by 50- μm alumina	10

TABLES

1. Regression coefficients, correlation coefficient, and exponents for each target material	5
2. Impingement angles of maximum and minimum wear taken from model plots of figures 4 through 15	7
3. Velocity exponent for each material calculated from velocity versus maximum specific wear at each velocity	11
B-1. Raw test data for effect of particle velocity and impingement angle on specific wear	14

UNIT OF MEASURE ABBREVIATIONS USED IN THIS REPORT

°C	degree Celsius	HRB	Rockwell B hardness
cm	centimeter	HRC	Rockwell C hardness
deg	degree	HV	Vicker's hardness
DPH	diamond pyramid hardness	lbm	pound-mass
ft-lbf/g	foot times pound-force per gram	mg	milligram
ft/s	foot per second	min	minute
g	gram	mm	millimeter
g/cm ³	gram per cubic centimeter	mm ³ /g	cubic millimeter per gram
g/min	gram per minute	μm	micrometer
h	hour	m/s	meter per second
HRA	Rockwell A hardness		

EROSIVE WEAR OF POTENTIAL VALVE MATERIALS FOR COAL-CONVERSION PLANTS

By L. Garner McDonald¹ and John E. Kelley²

ABSTRACT

The U.S. Bureau of Mines, under contract to the U.S. Department of Energy, investigated the erosive-wear properties of seven commercial alloys with potential applications as valves for coal-conversion plants.

A dry particle, jet-erosion apparatus was used to determine the wear of seven materials: 316 and 440-C stainless steels, K-68, K-701, and K-801 cemented tungsten carbides, HC-250 white cast iron, and Haynes 6B. The alumina abrasive entrained in the nitrogen gas jet had particle sizes of 27 or 50 μm , the abrasive velocities were 55 to 170 m/s, and the particle impingement angles were 15° to 90°.

The maximum specific wear for ductile materials was found to occur at impingement angles of 15° to 30°, and the minimum specific wear occurred at 60° to 90°. For the brittle materials, maximum specific wear occurred at impingement angles of 50° to 85° and minimum specific wear was at the lowest angles.

As the velocity and erosive particle size increased, the specific wear increased. The specific wear was related to the velocity by the power function $W \propto AV^n$, where n was 1.8 to 3.9 for ductile materials and 1.8 to 3.6 for brittle materials.

¹Metallurgist.

²Metallurgist (now with Advanced Surfaces and Processes, Inc., Cornelius, OR).
Albany Research Center, U.S. Bureau of Mines, Albany, OR.

INTRODUCTION

A major program in the Fossil Energy Division of the U.S. Department of Energy is the research and development of materials that can be used in valves that handle solids and liquids in coal-conversion plants. This report presents a study by the U.S. Bureau of Mines on the erosion characteristics of candidate valve materials. The study was funded through Interagency Agreement DE-A105-800R20687.

The successful operation of commercial coal-conversion plants depends on the adequate performance of valve components. Abrasives such as fly ash, slag, char, coke breeze, and coal are transferred through these valves in rapidly flowing gases and liquids. Several types of wear operate on these valves and valve parts, but the research reported here focused only on erosion by abrasive particles entrained in rapidly flowing gases.

Wear by hard particle cutting and gouging or wear by metal galling are the norm for lockhopper valves. Erosion from high-velocity particle flow in ash-laden gases can greatly accelerate valve damage. Figures 1 and 2 show erosive-wear damage on two valves taken from the Morgantown Energy Technology Low BTU Producer Gas Demonstration Plant. The 316 stainless steel ball and the Haynes 6 valve seat from a lockhopper valve are shown in figure 1. The worn channel most likely began as damage from galling or from a particle of ash or char jammed between the ball and seat. Once the leak channel was formed, fine abrasive particles entrained in the high-velocity gases rapidly produced the deeply eroded grooves.

The 316 stainless steel body of a pressure let-down, butterfly valve liner is shown in figure 2. Particulates in the product gas (called "coke breeze") were estimated to be traveling greater than 165 m/s through the valve. They severely eroded the tungsten carbide-coated steel butterfly and liner in 40 h of operation.

Many researchers have studied particle entrained abrasive wear (1-30).³ The factors most commonly evaluated are abrasive particle size, shape, hardness, velocity, impingement angle, target hardness, ductility, microstructure, work hardening, and strain-to-fracture. These factors are used to develop modern models of gas-entrained abrasive particle erosion. The models can be classified into three broad categories. The first model is for the ductility of the target. The second model is for impact angle (i.e., cutting, microfatigue, and microspalling). The third model is for angularity of the abrasive. In actuality, each category overlaps the other two categories. For example, the angularity of the abrasive can affect the angle where metal cutting decreases and microfatigue or microspalling begins to dominate.

To verify models, researchers have used target materials such as glass, hardened and annealed steels, hardened and annealed aluminum alloys, single crystals of pure copper, carbon, annealed and cold-rolled brass, and Perspex polycarbonate resin.⁴ They used specific angles of impingement (generally 90°) or a range of angles from 4° to 90°. Particle materials such as glass and steel spheres, angular silica sand, alumina, silicon carbide, tungsten carbide, and various mineral dusts have been used. The particles have ranged in size from 15 μm to 3 mm. Particle velocities have ranged from 15 to 450 m/s.

⁴Reference to specific products does not imply endorsement by the U.S. Bureau of Mines.

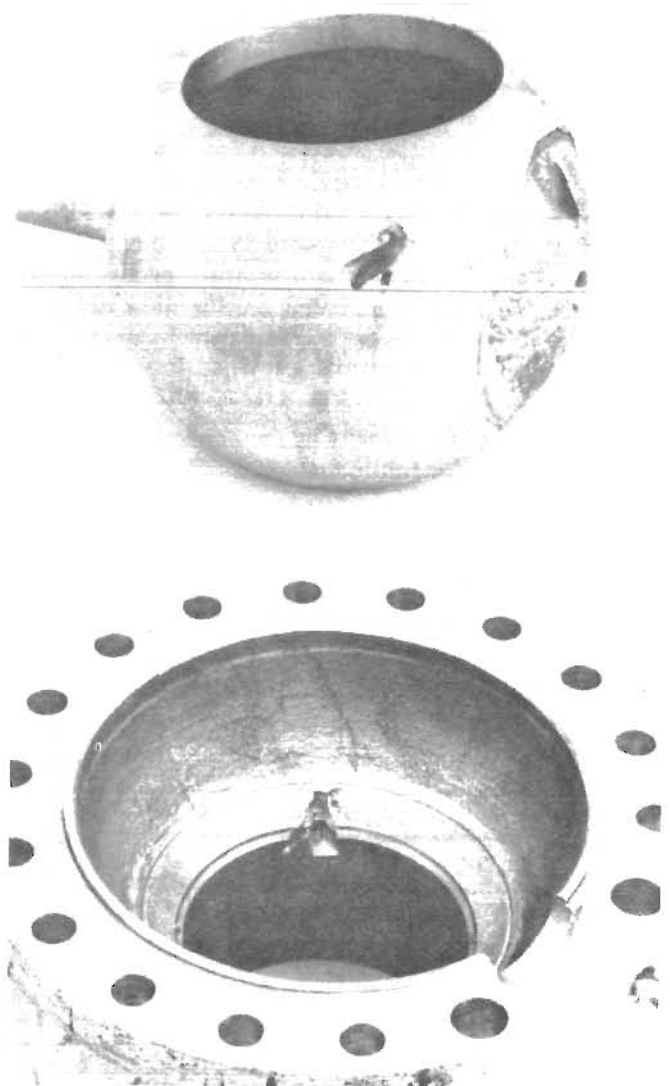


Figure 1.—Lockhopper ball-valve (top) and valve-seat (bottom) damaged by entrained particle erosion.

³Italic numbers in parentheses refer to items in the list of references preceding the appendixes at the end of this report.



Figure 2.—Let-down valve liner damaged by entrained particle erosion.

Erosive wear of a material can vary drastically because of several factors. For ductile materials, the angle of maximum wear is reported by many (6-7, 14, 18) to be about 20° . Depending on the target material, Smeltzer, Gulden, and Compton (8) found the maximum wear to occur between 30° and 37.5° using $5\text{-}\mu\text{m}$ Al_2O_3 particles at a velocity of 152 m/s. Head and Harr (7) reported maximum wear of an aluminum alloy at 45° when eroded with glass beads. Neilson and Gilchrist (6) reported a maximum wear rate at 45° on Perspex polycarbonate resin for $210\text{-}\mu\text{m}$ alumina abrasive at 130 m/s. Mills and Mason (14) reported a maximum wear rate at 20° for mild steel. They also reported maximum penetration occurred between 45° and 60° .

For "simple-structure" brittle materials such as ceramics, maximum wear usually occurs at normal incidence (90°). However, Sheldon (2, 4) found that under certain conditions the erosion-wear impingement angle relationship for a brittle material approaches that of a ductile material. He showed that with 1,000-mesh particles, brittle material erosion behavior became indistinguishable from ductile behavior.

A particle in motion possesses kinetic energy that can damage the surface of a target material upon impact. Since the kinetic energy is proportional to the particle mass and the square of the particle velocity, one could expect the quantity of damage to be proportional to the mass and square of the velocity. Finnie, Kabil, and Wolak (5) reported that erosive wear is proportional to a power function of the velocity. The exponent can be as high as

2.4 for ductile materials. Goodwin, Sage, and Tilly (9) reported an exponent of 2 to 2.3. For brittle materials, Sheldon (2) found the velocity exponent to be as high as 4.4.

Most researchers have found that wear increases with increased particle size, all other factors being the same, but published erosion wear data show some disagreement. Finnie (10) found that particle size had no effect above $150\text{ }\mu\text{m}$ for ductile target metals, while Head and Harr (7) reported that the erosion of carbides increased with particle size up to $300\text{ }\mu\text{m}$, and thereafter decreased up to $900\text{ }\mu\text{m}$. Sheldon (2) noted no size effect on aluminum for 51-, 125-, and $250\text{-}\mu\text{m}$ particles, but for smaller particles, he reported decreased erosion. Brown, Jun, and Edington (20) concluded that erosion rates in $\alpha\text{-Fe}$ increased rapidly with particle size until the fracture of the spherical glass particles occurred. Goodwin, Sage, and Tilly (9) found that there is a critical size above which erosion rate is no longer affected and that the critical size varies linearly with particle velocity. Mills and Mason (14) reported a difference in the type of erosion damage caused by $70\text{-}\mu\text{m}$ sand versus $210\text{-}\mu\text{m}$ sand on a mild steel target. The large particles removed more overall mass from the target than the smaller particles, but the smaller ($70\text{-}\mu\text{m}$) particles cut deeper and narrower paths than did the $210\text{-}\mu\text{m}$ particles.

Generally, the amount of material removed by erosion is directly proportional to the amount of abrasive impinging on the surface. However, high concentrations of erosive particles usually result in decreased erosion-wear efficiency because some of the particle energy is expended in colliding with other particles. At low particle concentrations, Wood and Espenshade (3), Smeltzer, Gulden, and Compton (8), and Young and Ruff (13) all reported greater erosion-wear efficiency per particle.

Particle hardness normally is considered to have little influence on erosion wear of ductile materials provided the particles are harder than the target material. Finnie, Kabil, and Wolak (5) found erosion rate increased as a function of Vicker's hardness for the particles at low angles. Levy and Chik (26) reported that erosion rate no longer increased with particle hardness after 700 HV. On the other hand, Goodwin, Sage, and Tilly (9) report that wear is a function of diamond pyramid hardness to the power of 2.3 for many target materials when angles of 20° to 90° were used with sand abrasive. The shape of particles usually has more effect on erosion than hardness. Sharp particles produce greater erosion wear than rounded particles.

Under most operating conditions, total erosive wear is linear with time. Exceptions are short-time break-in effects and long-time geometric effects when the actual impingement angle differs from the apparent impingement angle because of the development of a crater in the target material (14).

It is difficult to express reliable correlations of erosion resistance of materials with other material properties. Finnie, Kabil, and Wolak (5) found that erosion wear is constant for different hardnesses of the same steel alloy. Smeltzer, Gulden, and Compton (8) reported that differing heat treatments on 2024 aluminum, 17-7 PH stainless steel, 410 stainless steel, and Ti-6Al-4V alloys had no effect on erosion wear. Finnie (15) suggested flow stress as a universal property to predict erosion resistance in ductile materials. In addition, Smeltzer, Gulden, and Compton (8) and Head and Harr (7) have shown some correlation of erosion wear with elastic modulus and melting point.

Although previous researchers have done substantial work, erosion problems in coal gasification valves remain formidable. The complex nature of the problem is such

that a change in any one of several variables affecting erosion may render a material satisfactory in one application but unsuitable in another. Researchers have developed several relationships to equate the variables to physical properties (4-8). However, design engineers, needing materials selection guidance, have found the equations to be of little practical significance. The equations apply only to narrow classes of materials and involve difficult-to-measure properties, all variables are not accounted for in any one equation, and special tests are required for the determination of constants. Each empirical three-dimensional graph presented in this report is target material specific and should prove applicable to estimating the amount of wear over a range of impingement angles and particle velocities.

ACKNOWLEDGMENTS

The authors gratefully acknowledge the assistance of C. Lyle Hoatson, Tu Tan Mai, and Deborah J. Singleton, who conducted the experimental studies. The computer graphics and data entry were done by Brent Madsen and

Ellen Mattlin, Sophie J. Bullard, Bernard S. Covino, Jr., and Gordon Holcomb helped by improving the quality of both the graphics and the text.

CURVE-FIT EQUATIONS FOR THREE-DIMENSIONAL PLOTS

The model developed herein evolved as a means to construct three-dimensional plots based on the kinetic energy model of Neilson and Gilchrist (6). Neilson and Gilchrist hypothesize that at low impingement angles the impacting particles are predominantly performing cutting wear and at high impingement angles the impacting particles are predominantly performing deformation wear. Furthermore, at low angles some particles glance off the surface, thereby imparting only a portion of their kinetic energy to cutting wear and for hard target materials there is a minimum velocity below which no deformation wear occurs. The Neilson and Gilchrist model produces the following equations to describe gas-entrained abrasive wear:

$$W = \frac{1/2M (V\sin\alpha - V_k)^2}{\xi} + \frac{1/2MV^2\cos^2\alpha\sin(n\alpha)}{\phi} \text{ for } \alpha < \alpha_0, \quad (1)$$

$$\text{and } W = \frac{1/2M (V\sin\alpha - V_k)^2}{\xi} + \frac{1/2MV^2\cos^2\alpha}{\phi} \text{ for } \alpha = \alpha_0, \quad (2)$$

- where
- W = erosive wear (g);
 - M = mass of a particle (lbm);
 - V = particle velocity (ft/s);
 - α = angle of particle impingement measured with respect to the target surface; 0° is parallel and 90° is perpendicular to the surface;
 - α_0 = angle of impingement above which there are no more glancing impacts;
 - ξ = kinetic energy absorbed by surface to produce one unit of eroded material by deformation wear (ft-lbf/g);
 - ϕ = kinetic energy absorbed by surface to produce one unit of eroded material by cutting wear (ft-lbf/g);
 - V_k = normal velocity component below which no deformation wear occurs (ft/s);

$\sin n\alpha$ = compensating factor for the parallel kinetic energy component so that there is a loss in cutting wear at low impingement angles where glancing impacts occur;

and n = constant such that $\sin n\alpha_o = 1$.

The Neilson and Gilchrist model was simplified for utilization in this report as follows:

$$W = 1/2MV^A \sin^B \alpha + 1/2MV^C \cos^D \alpha \sin^E \alpha \text{ for } 0 \leq \alpha \leq \pi/2, \quad (3)$$

where W = specific wear (10^{-3}mm^3 target per gram abrasive);

V = particle velocity (m/s);

α = impingement angle (radians);

A, B, C, D, E = exponents calculated for each target material for each of the two particle sizes ($27 \mu\text{m}$ and $50 \mu\text{m}$) by iterative regression analysis to maximize the correlation coefficient, R ;

and M = individual mass of an abrasive particle (g).

M was approximated by

$$M = \frac{4\pi}{3} R^3 \rho,$$

particle mass (calculated to be $41.2 \times 10^{-9} \text{g}$ for the $27\text{-}\mu\text{m}$ particles and $261.8 \times 10^{-9} \text{g}$ for the $50\text{-}\mu\text{m}$ particles),

where R = approximate particle radius ($13.5 \mu\text{m}$ and $25 \mu\text{m}$);

and ρ = density of alumina (4g/cm^3).

In comparing the Neilson and Gilchrist model with the model above, the first term of the equations primarily describes the deformation wear and the second term describes cutting wear. The target material factors, ξ and ϕ , are not required because each three-dimensional plot (specific wear versus V versus α) is target material and particle size specific. Also, the exponents (B and E) on the trigonometric (sine) terms are an empirical compensation for any minimum velocity component required for deformation wear and the reduction in cutting wear due to glancing, respectively.

The final generalized equation that was used to analyze the erosion wear data and produce the three-dimensional plots is

$$W = q_0 + q_1 \left[\frac{1}{2} MV^A \sin^B \alpha \right] + q_2 \left[\frac{1}{2} MV^C \cos^D \alpha \sin^E \alpha \right]. \quad (4)$$

Table 1 shows the values calculated for the regression coefficients ($q_0, q_1,$ and q_2), the correlation coefficient (R), and the exponents ($A, B, C, D,$ and E) for each material and particle size.

Table 1.—Regression coefficients ($q_0, q_1,$ and q_2), correlation coefficient (R), and exponents ($A, B, C, D,$ and E) for each target material

Abrasive and target material	q_0	q_1	q_2	R	A	B	C	D	E
27- μm alumina:									
316 stainless steel	6.06	144,802	288,681	0.98	2.1	2.9	2.3	5.0	0.8
440-C stainless steel, annealed	4.18	3,588	128,754	.99	2.8	3.1	2.4	4.2	.8
440-C stainless steel, hardened	1.55	284,769	161,965	.99	2.0	2.4	2.4	3.8	.9
HC-250 white cast iron	3.44	58,604	199,059	.99	2.3	3.5	2.3	3.3	1.0
Haynes 6B	2.81	153,341	2,296,387	.99	2.1	3.0	1.8	3.2	.8
K-68 cemented WC	.24	25,106	73,302	.99	2.2	2.2	1.8	.4	2.2
50- μm alumina:									
316 stainless steel	4.63	6.8524	221.89	.98	3.9	3.0	3.5	4.2	.7
440-C stainless steel, annealed	2.40	28.859	66.291	.98	3.6	3.5	3.7	3.1	.6
HC-250 white cast iron	3.85	242.35	4726.2	.995	3.2	.3	2.7	4.1	.8
Haynes 6B	8.41	.6423	472.54	.98	4.4	.3	3.2	4.0	1.0
K-701 cemented WC	.02	8.2599	118.08	.99	3.6	4.5	2.9	1.4	.9
K-801 cemented WC	.07	5494.2	178.31	.98	2.1	1.9	2.9	1.4	1.1

TEST EQUIPMENT

The erosion tests (31) were performed at room temperature on equipment shown in figure 3. An S.S. White Model H Airbrasive unit was used to mix the alumina particles into a nitrogen gas stream and control the particle flow rate and velocity. The particle-gas mixing was done in a pressurized hopper mounted on a vibrator within the Airbrasive unit. An orifice in the hopper controlled the flow of particles into the gas stream, and the particle flow rate was controlled by adjusting the voltage applied to the hopper vibrator. Particle velocity was controlled by gas stream pressure, and was calibrated periodically on a rotating dual-disk device as described by Ruff and Ives (12).

Two different nozzles were used in the tests. One, a sapphire tube, had an inside diameter of 0.58 mm and was 1.3 cm long. The 27- μm particles were blown through this nozzle. The other nozzle was a cobalt-bonded tungsten carbide tube 5.3 cm long with a bore of 1.5 mm. The 50- μm particulates were blown through the second nozzle. The inside diameter and not the material is the only significance of using two different nozzles. The distance between the end of the nozzle and the specimen surface was set at 1 cm. The particle flow rates and velocities were different for each nozzle. Because of this, the data for these nozzles are presented separately throughout this report.

Particle impingement angles were set to the desired angle by adjusting the sample holder, as shown in figure 3. A hole through the sample holder beneath the sample was connected to a vacuum pump to hold the sample in place during the erosion test. The sample holder and nozzle assembly were placed under an exhaust hood equipped with a dust filter.

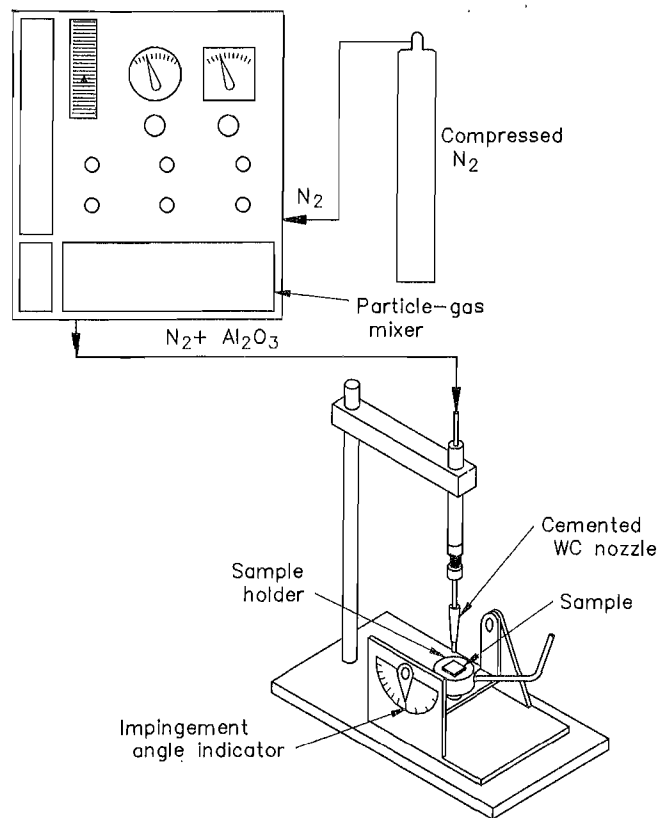


Figure 3.—Erosion test equipment.

MATERIALS

Seven commercial materials (32-35) were studied for use in valves for coal conversion plants. These materials were 316 austenitic stainless steel, annealed and hardened 440-C martensitic stainless steel, HC-250 high-chromium white cast iron, Haynes 6B cobalt-based superalloy, and

three grades of cemented tungsten carbides (K-68, K-701, and K-801). A description of each material is given in appendix A. All of the tests were made with two sizes of angular Al_2O_3 particles, 27 μm and 50 μm diameter. Virgin Al_2O_3 particles were used for each test.

PROCEDURES

The erosion samples were 1.3 by 1.3 by 0.2 cm, or 1.3 by 1.9 by 0.2 cm. All of the samples, except cemented tungsten carbides, were ground and polished by hand on SiC papers from 60 grit through 600 grit before testing. The as-received surface condition of the cemented tungsten carbide samples was already smoother than a 600-grit polish.

The powder flow-rate was verified by measuring it before and after each wear test. When a difference greater than 10% in powder flow-rate was noted, the test was considered to be invalid and the results were not used. Powder flow-rates were measured by aiming the nozzle into a long glass tube sealed by stoppers, one of which had a gas vent and a nozzle hole. The abrasive powder

caught in the tube was weighed and a rate calculated by dividing the weight by the number of minutes of flow. Independent of the gas velocity, the abrasive powder flow-rate was approximately 3 g/min for 27- μm data and 2 g/min for the 50- μm data. The particulate mass used in each test to abrade the target was collected in a gas-particle separator and accurately weighed; thus the need for exact powder flow-rate control from test to test was not necessary.

Prior to testing, the eroding gas-particle stream was directed onto the sample for 1 to 3 min, depending on target material, to minimize the effects of break-in. Then each sample was washed in acetone in an ultrasonic cleaning tank, dried in a warm air blast, and weighed on a balance with ± 0.1 mg precision. After break-in conditions were established, the actual test was run with durations from 3 to 10 min, depending on target material. At the end of an erosion test, the sample was again washed, dried, and weighed. Target material losses of less than 4 mg in a test were found to decrease the reproducibility. The mean

weight loss value, averaged for two to five tests on a given material and for a given set of test conditions, was divided by the density of target material to determine the volume of material lost due to erosion wear. This value was then divided by the mean weight of abrasive powder used to erode this material to determine a specific wear (cubic millimeters per gram). The specific wear corresponds to the volume of target material lost due to the erosive action of 1 g of abrasive powder.

For the 27- μm -abrasive data group, the Al_2O_3 powder was screened twice within a very narrow particle size range of -37 μm +20 μm . Erosive wear data were collected for six different impingement angles between 15° and 90° at four velocities of 75, 95, 115, and 170 m/s. For the 50- μm -abrasive data group, the Al_2O_3 powder was screened twice within a very narrow particle size range of -63 μm +44 μm . These tests also were made at six impingement angles between 15° and 90°, and at velocities of 55, 65, 75, 85, 105, and 115 m/s.

RESULTS AND DISCUSSION

The correct understanding of the brittle or ductile nature of a material is important. For instance, a hardened steel or white cast iron that is normally considered to behave in a brittle manner in terms of impact resistance may behave in a ductile manner in terms of erosion wear. Also, data given for only one angle may lead to false impressions of the total erosion-wear behavior of a material. That is why this report includes the behavior of several materials over a range of impingement angles and particle velocities. Three-dimensional curves of specific wear versus particle velocity and impingement angle for 27- μm and 50- μm abrasives are displayed in figures 4 through 15. Raw erosive-wear data are given in appendix B.

PARTICLE IMPINGEMENT ANGLE EFFECTS

With the exception of the cemented tungsten carbides, the raw data for the metal alloys showed maximum wear at 15° to 30° and minimum wear at 90°. The kinetic energy model (table 2) gives maximum wear at 24° to 36° and minimum wear at 60° to 90°. The raw data for the cemented tungsten carbides, shown in appendix B, showed maximum wear at 45° to 90° and minimum wear at the lowest angle. The model showed maximum wear at 48° to 84° and minimum at the lowest angle. A tabular summary of the angles of maximum and minimum erosion wear at different particle velocity ranges are shown in table 2.

Table 2.—Impingement angles of maximum and minimum wear taken from model plots of figures 4 through 15

Abrasive and target material	Maximum wear angle, deg, at each velocity range					Minimum wear angle, deg, at each velocity range				
	55-65 m/s	75-85 m/s	95-105 m/s	115 m/s	170 m/s	55-65 m/s	75-85 m/s	95-105 m/s	115 m/s	170 m/s
27- μm Al_2O_3 :										
316 stainless steel	24	24	24	24	24	66	66	60	60	60
440-C stainless steel, annealed	24	24	24	24	24	72	66	66	66	66
440-C stainless steel, hardened	30	30	30	30	30	66	66	66	66	66
HC-250 white cast iron	30	30	30	30	36	66	66	66	66	66
Haynes 6B	30	30	30	30	30	78	78	72	72	72
K-68 cemented WC	78	78	78	78	84	90	90	90	90	90
50- μm Al_2O_3 :										
316 stainless steel	24	24	24	24	24	24	72	66	66	66
440-C stainless steel, annealed	30	24	24	24	24	72	72	72	72	72
HC-250 white cast iron	24	24	30	30	36	90	90	84	84	84
Haynes 6B	30	30	30	30	30	78	84	84	8	84
K-701 cemented WC	66	66	60	60	60	90	90	90	90	90
K-801 cemented WC	48	48	48	54	54	90	90	90	90	90

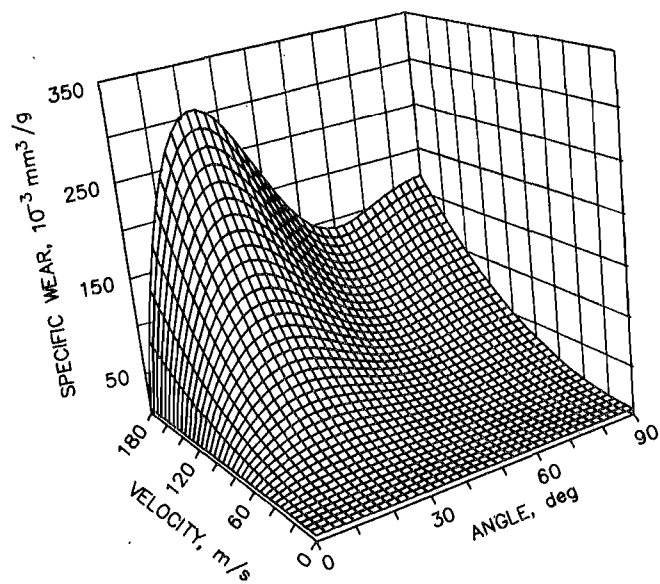


Figure 4.—Effect of velocity and impingement angle on specific wear of 316 stainless steel eroded by 27-μm alumina.

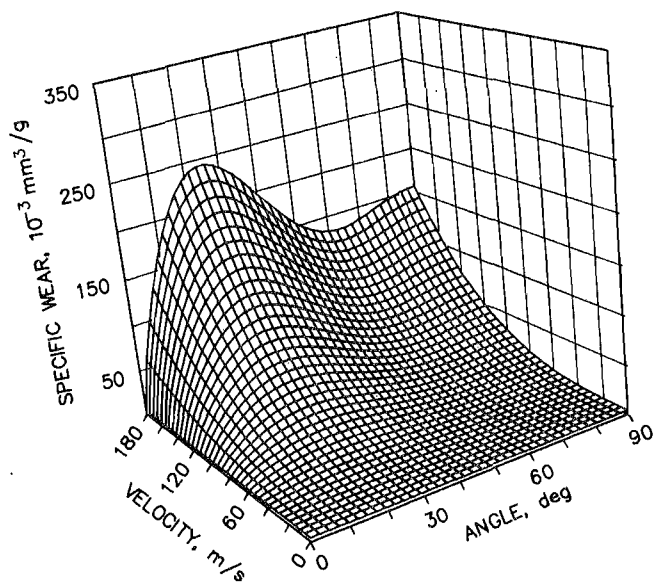


Figure 5.—Effect of velocity and impingement angle on specific wear of annealed 440-C stainless steel eroded by 27-μm alumina.

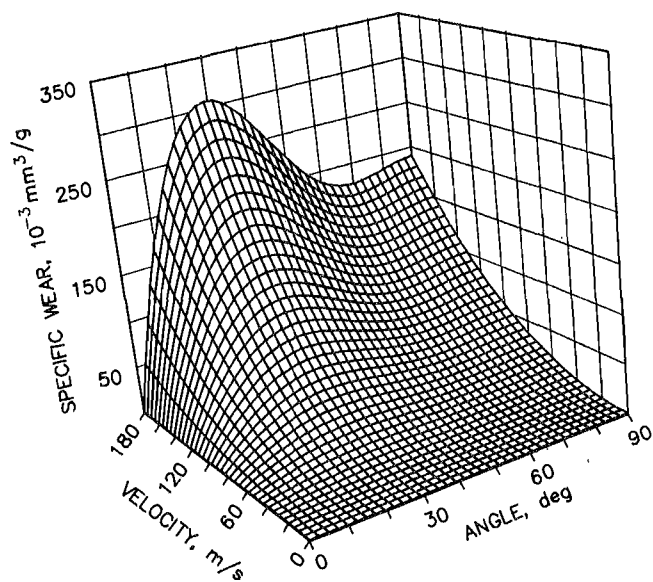


Figure 6.—Effect of velocity and impingement angle on specific wear of hardened 440-C stainless steel eroded by 27-μm alumina.

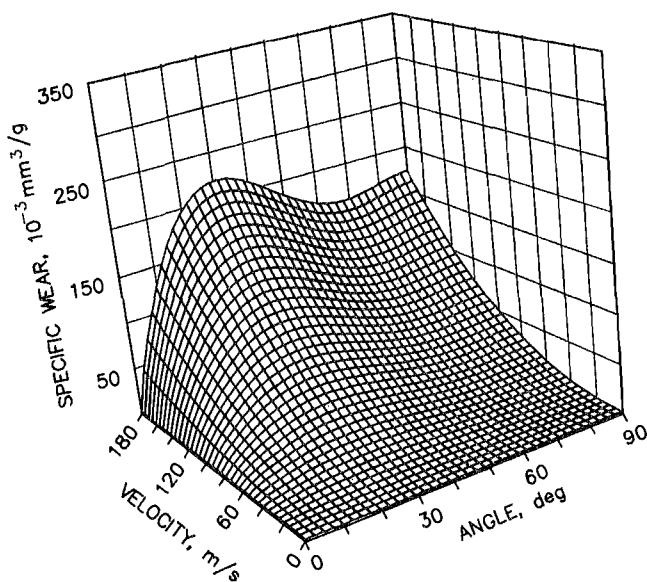


Figure 7.—Effect of velocity and impingement angle on specific wear of HC-250 white cast iron eroded by 27-μm alumina.

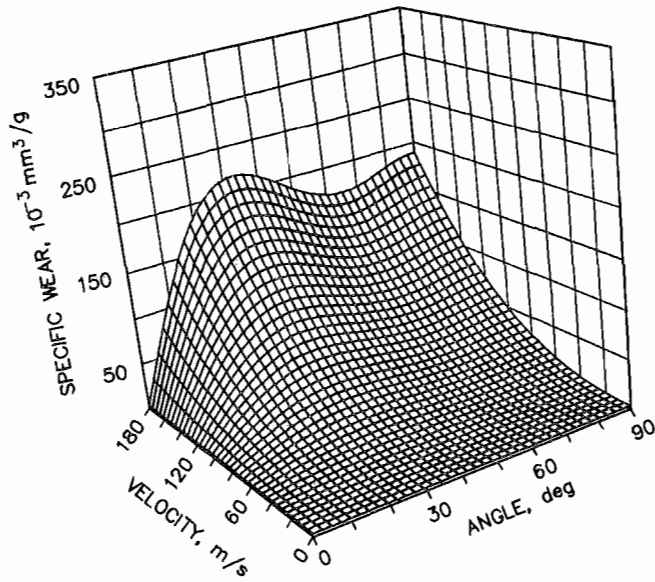


Figure 8.—Effect of velocity and impingement angle on specific wear of Haynes 6B cobalt-based superalloy eroded by 27- μm alumina.

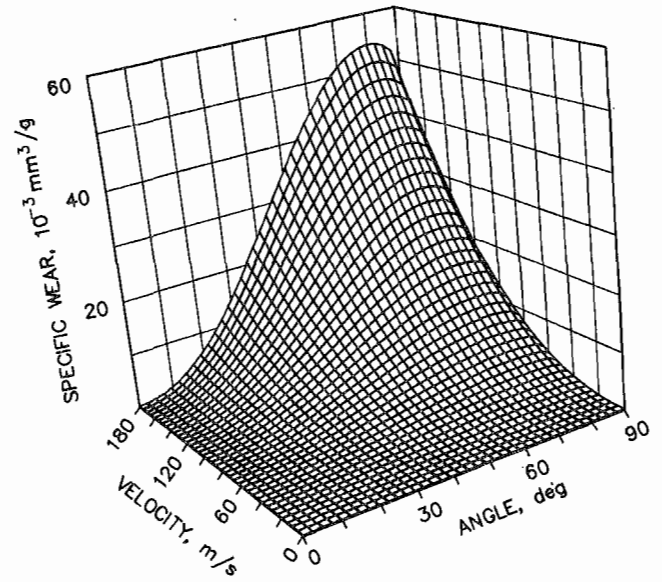


Figure 9.—Effect of velocity and impingement angle on specific wear of K-68 cobalt-bonded tungsten carbide eroded by 27- μm alumina.

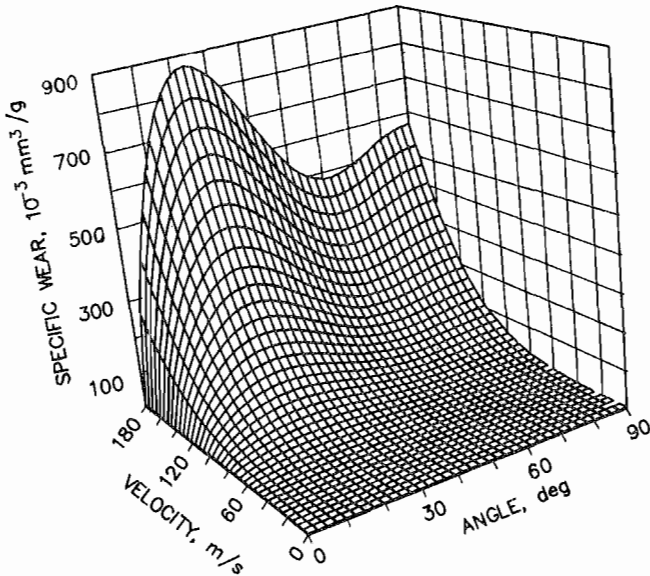


Figure 10.—Effect of velocity and impingement angle on specific wear of 316 stainless steel eroded by 50- μm alumina.

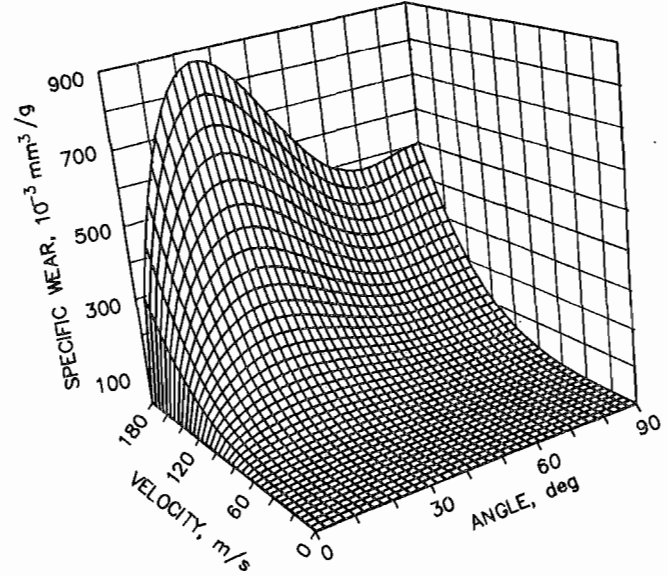


Figure 11.—Effect of velocity and impingement angle on specific wear of annealed 440-C stainless steel eroded by 50- μm alumina.

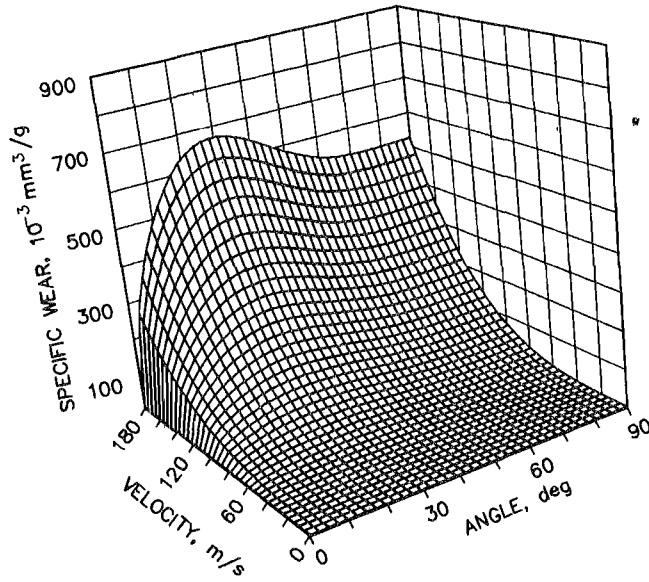


Figure 12.—Effect of velocity and impingement angle on specific wear of HC-250 white cast iron eroded by 50- μ m alumina.

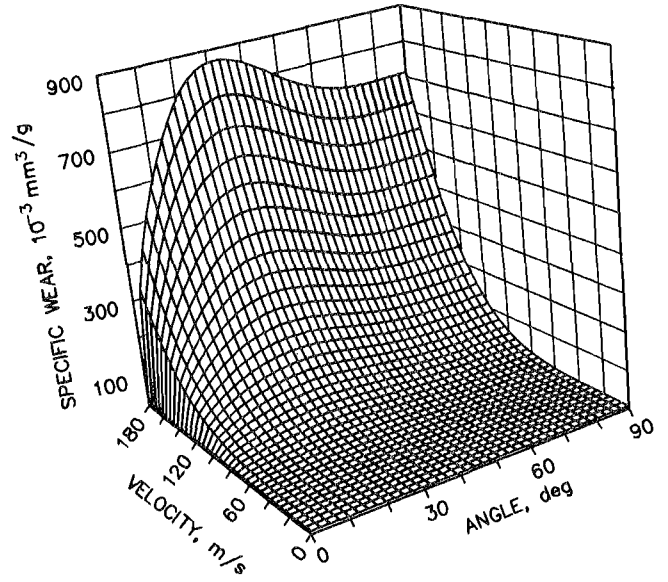


Figure 13.—Effect of velocity and impingement angle on specific wear of Haynes 6B cobalt-based superalloy eroded by 50- μ m alumina.

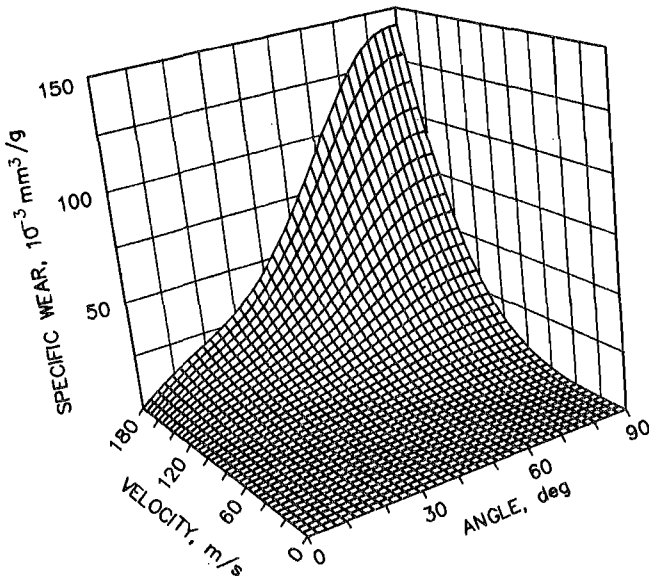


Figure 14.—Effect of velocity and impingement angle on specific wear of K-701 cobalt and chromium-bonded tungsten carbide eroded by 50- μ m alumina.

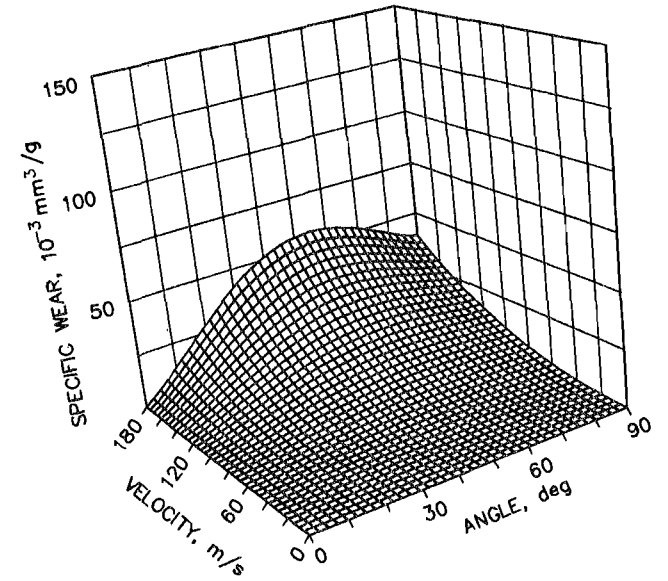


Figure 15.—Effect of velocity and impingement angle on specific wear of K-801 nickel-bonded tungsten carbide eroded by 50- μ m alumina.

Due to the relatively short durations of the tests, little or no cratering was observed. Thus, the geometrical effects to the impingement angle from cratering, as described by Mills and Mason (14), were negligible.

PARTICLE VELOCITY EFFECTS

For the erosion-wear data presented in this report, the velocity exponents (table 3) were lower for tests with 27- μm Al_2O_3 than with 50- μm Al_2O_3 . The velocity exponent for each material at the maximum wear angle calculated from the relation "wear $\propto V^n$ " (V = particle velocity and n = velocity exponent) is shown in table 3. Exponents calculated for velocity in the kinetic energy model are given as A and C in table 1.

Velocity exponents at the maximum wear angle, table 3, ranged from 1.7 to 3.5 for metals and from 1.8 to 2.6 for the more brittle cemented carbides. Model values, table 1, show the exponents ranging from 1.8 to 3.9 for the metals and 1.8 to 3.6 for the cemented carbides.

SUMMARY

There are many factors that affect the erosive-wear behavior of a material eroded by a gas-entrained abrasive. The two factors stressed by this research are particle impingement angle and particle velocity. Some other factors not covered by the experimental testing but still discussed in the report are particle size; particle shape; particle flux; relative hardness between the abrasive and the target; erosion time; and target material characteristics such as flow stress, melting point, and elastic modulus.

For the ductile materials, a maximum specific wear is obtained at angles between 15° and 30° in the raw data and 24° and 36° in the kinetic energy model, followed by a decline to lower values with increasing angle. Minimum wear is obtained at angles of 90° for the raw data and between 60° and 90° for the model. For the brittle materials, such as the cemented tungsten carbides, the raw data gave maximum specific wear values near 60° to 65° and the model predicted maximum values between 48° and 84° depending on the target material and particle size, and a shallow minimum at 90°.

The relationship found between particle velocity and wear rate confirms the observations of other investigators that wear rate is proportional to a power function of the velocity for both ductile and brittle target materials. These

Table 3.—Velocity exponent (n) for each material calculated from velocity versus maximum specific wear at each velocity (wear $\propto V^n$)

<i>Abrasive and target material</i>	<i>n</i>
<i>27-μm Al_2O_3 particles:</i>	
316 stainless steel	1.7
440-C stainless steel, annealed	2.3
440-C stainless steel, hardened	2.4
HC-250 white cast iron	2.0
Haynes 6B	1.7
K-68 cemented wc	1.9
<i>50-μm Al_2O_3 particles:</i>	
316 stainless steel	2.3
440-C stainless steel, annealed	3.5
H-250 white cast iron	2.8
Haynes 6B	3.3
K-701 cemented WC	1.8
K-801 cemented WC	2.6

investigators show the exponent of the function to be as high as 2.4 for ductile materials and 4.4 for brittle materials. For ductile target materials, the research reported here yields exponent values 1.8 to 3.9. For brittle materials, the exponent values were 1.8 to 3.6. Also, for each target material, the velocity exponents are usually lower for the 27- μm alumina particles than the 50- μm particles.

The kinetic energy model that was constructed to draw three-dimensional plots of specific wear proved to be useful for predicting the angles of maximum and minimum wear rates as well as the exponents on the velocity power functions. However, limitations in the model were found for the higher particle velocities on the ductile materials. The model predicts local minimums in the wear rate between 60° and 90°, in contrast to the minimums found at 90° in the raw data.

At high velocities, the particle size effect found in this research is consistent with the results of other investigators. The wear rate increases with the increase in particle size from 27 to 50 μm . At low velocities, however, the effect of particle size, as determined by this research, is reversed from the conclusions of most other investigators. The wear rate is higher for the smaller, 27- μm , particles than it is for the larger, 50- μm , particles.

REFERENCES

1. Finnie, I. Erosion of Surfaces by Solid Particles. *Wear*, v. 3, 1960, pp. 87-103.
2. Sheldon, G. L. Erosion of Brittle Materials. Ph.D. Thesis, Univ. of CA, Berkeley, CA, 1965, 233 pp.
3. Wood, C. D., and P. W. Espenshade. Mechanisms of Dust Erosion. *SAE Trans.*, v. 73, Aug. 1965, pp. 515-523.
4. Sheldon, G. L., and I. Finnie. The Mechanism of Material Removal in the Erosive Cutting of Brittle Materials. *Trans. ASME*, v. 88B, 1966, pp. 387-392.
5. Finnie, I., Y. Kabil, and J. Wolak. Erosion of Metals by Solid Particles. *J. Mater.*, v. 2, No. 3, Sept. 1967, pp. 682-700.
6. Neilson, J. H., and A. Gilchrist. Erosion by a Stream of Solid Particles. *Wear*, v. 11, 1968, pp. 111-122.
7. Head, W. J., and M. E. Harr. The Development of a Model To Predict the Erosion of Materials by Natural Contaminants. *Wear*, v. 15, 1970, pp. 1-46.
8. Smeltzer, C. E., M. E. Gulden, and W. A. Compton. Mechanisms of Metal Removal by Impacting Dust Particles. *J. Basic Eng.*, v. 92, 1970, pp. 639-654.
9. Goodwin, J. E., W. Sage, and G. P. Tilly. Study of Erosion by Solid Particles. *Proc. Inst. Mech. Eng.*, v. 184, pt. 1, No. 15, 1970, pp. 279-291.
10. Finnie, I. Some Observations on the Erosion of Ductile Metals. *Wear*, v. 19, 1972, pp. 81-90.
11. Head, W. J., L. D. Lineback, and C. R. Manning. Modification and Extension of a Model for Predicting the Erosion of Ductile Materials. *Wear*, v. 23, 1973, pp. 291-298.
12. Ruff, A. W., and L. K. Ives. Measurement of Solid Particle Velocity in Erosive Wear. *Wear*, v. 35, 1975, pp. 195-199.
13. Young, J. P., and A. W. Ruff. Particle Erosion Measurements on Metals. *J. Eng. Mater. and Technol.*, v. 99, No. 2, Apr. 1977, pp. 121-125.
14. Mills, D., and J. S. Mason. Particle Size Effects in Bend Erosion. *Wear*, v. 44, 1977, pp. 311-328.
15. Finnie, I. The Mechanism of Erosion of Ductile Materials. *Proceedings of the 3rd Material Congress of Applied Mechanics, AIME (New York, 1958)*. Pergamon, 1978, pp. 527-532.
16. Hansen, J. S., J. E. Kelley, and F. W. Wood. Erosion Testing of Potential Valve Materials for Coal Gasification Systems. *BuMines RI 8335*, 1979, 26 pp.
17. Gupta, R. D. Super Hard Materials for Erosion Resistance: Status of Indigenous Development. *Nat. Met. Lab. Tech. J.*, India, v. 21, 1979, pp. 11-14.
18. Carter, G., M. J. Nobes, and K. I. Arshak. The Mechanism of Ripple Generation on Sand-Blasted Ductile Solids. *Wear*, v. 65, 1980, pp. 151-174.
19. Brown, R., and J. W. Edington. Erosion of Copper Single Crystals Under Conditions of 90° Impact. *Wear*, v. 69, 1981, pp. 369-382.
20. Brown, R., E. J. Jun, and J. W. Edington. Erosion of α -Fe by Spherical Glass Particles. *Wear*, v. 70, 1981, pp. 347-363.
21. Brown, R., and J. W. Edington. Subsurface Defect Structure of Eroded Copper Single Crystals. *Wear*, v. 72, 1981, pp. 377-386.
22. _____. Mechanisms of Material Loss During the Threshold Period of Erosion by Solid Particles. *Wear*, v. 77, 1982, pp. 347-353.
23. _____. Erosion of Copper Single Crystals Under Conditions of 30° Incidence. *Wear*, v. 79, 1982, pp. 335-346.
24. Brown, R., S. Kosco, and E. J. Jun. The Effect of Particle Shape and Size on Erosion of Aluminum Alloy 1100 at 90° Impact Angles. *Wear*, v. 88, 1983, pp. 181-193.
25. Cousens, A. K., and I. M. Hutchings. A Critical Study of the Erosion of an Aluminum Alloy by Solid Spherical Particles at Normal Impingement. *Wear*, v. 88, 1983, pp. 335-348.
26. Levy, A. V., and P. Chik. The Effects of Eroderent Composition and Shape on the Erosion of Steel. *Wear*, v. 89, 1983, pp. 151-162.
27. Naim, M., and S. Bahadur. The Significance of the Erosion Parameter and the Mechanisms of Erosion in Single-Particle Impacts. *Wear*, v. 94, 1984, pp. 219-232.
28. Emiliani, M. R., and R. Brown. The Effect of Microstructure on the Erosion of Ti-6Al-4V by Spherical Particles at 90° Impact Angles. *Wear*, v. 94, 1984, pp. 323-338.
29. Carter, G., and M. J. Nobes. A Kinematic Wave Description of Ripple Development on Sand-Blasted Ductile Solids. *Wear*, v. 96, 1984, pp. 227-238.
30. Naim, M., and S. Bahadur. Work Hardening in Erosion Due to Single-Particle Impacts. *Wear*, v. 98, 1984, pp. 15-26.
31. American Society for Testing and Materials. Standard Practice for Conducting Erosion Tests by Solid Particle Impingement Using Gas Jets. G76-83 in 1984 Annual Book of ASTM Standards: Volume 3.02, Metal Corrosion, Erosion, and Wear. Philadelphia, PA, 1984, pp. 438-445.
32. American Society for Metals. Source book on Stainless Steels, 1976, pp. 386-388.
33. Avery, H. S. Work Hardening in Relation to Abrasion Resistance. *Proceeding of Symposium on Materials for the Mining Industry (Vail, CO, July 1974)*. Climax Molybdenum, A Division of AMAX, Inc., 1974, p. 70.
34. Cabot Corp., Haynes Div. Haynes Wrought Wear-Resistant Alloys. 1977, 20 pp.
35. Lucas, J. P. Valve Materials Performance Observed in Bench and Simulated Coal Gasification/Liquefaction Testing. Sandia Report No. SAND82-2363, May 1983, pp. 19-25.

APPENDIX A.—COMMENTS ON MATERIALS

1. *Type 316 Stainless Steel*

This is an austenitic corrosion-resistant stainless steel (32) (maximum composition: 0.08C, 2.0Mn, 0.045P, 0.030S, 1.0Si, 18.0Cr, 14.0Ni, 3.0Mo, Rem Fe). It is used in valve bodies and trim, especially for acid handling. The abrasion resistance and erosion resistance are fair, but galling resistance is poor. Type 316 stainless steel can only be hardened by cold working. The maximum service temperature is 870° C, and the scaling temperature in air is 900° C.

2. *Type 440-C Stainless Steel*

This is a hardenable martensitic high-carbon stainless steel (32) (maximum composition: 1.2C, 1.0Mn, 1.0Si, 0.040P, 0.030S, 18.0Cr, 0.75Mo, Rem Fe). The alloy is designed to provide a combination of high resistance to corrosion and wear, and to have high strength. The maximum operating temperature is 760° C. The alloy has been used successfully for ball-valve trim. The erosion resistance is fair.

3. *HC-250*

This alloy is a hardenable high-chromium white cast iron (33) (composition: 2.8C, 28.0Cr, Rem Fe). The structure is a martensite-austenite matrix containing chromium carbides. This alloy is used for components of abrasive slurry handling equipment. The abrasion resistance is very good to 540° C, and corrosion resistance to acids is good to 870° C.

4. *Haynes 6B*

This is a wrought cobalt-based superalloy (34) (composition: 1.2C, 2.0Mn, 2.0Si, 3.0Fe, 30.0Cr, 3.0Ni, 1.5Mo, 5.0W, and Rem Co). The alloy was developed for high resistance to corrosion and wear and is often used for valve trim. The erosion resistance is fair.

5. *K-68*

This is a cemented tungsten carbide material (35) containing 5.8% Co binder and the remainder WC. This material is often used for high-pressure pistons, wear guides, nozzles, and metal machining tool bits. It has good impact and compressive strength and excellent abrasion and erosion resistance.

6. *K-701*

This is a cemented tungsten carbide (35) with 10.2% Co plus 4.0% Cr binder and the remainder WC. The material is used for valve trim in slurry systems and in dirty-gas let-down valves. It was developed for high-wear and corrosion-resistant applications, and has excellent impact strength because of the binder content.

7. *K-801*

This is a cemented tungsten carbide (35) with 6% Ni binder and the remainder WC. It is commonly used for seal rings and valve trim for nuclear applications where cobalt (the usual binder) is undesirable. It has high wear and corrosion resistance, and is considered one of the strongest of the corrosion-wear grades.

APPENDIX B.—TEST DATA

Table B-1.—Raw test data for effect of particle velocity and impingement angle on specific wear

Target material	Abrasive velocity, m/s	Specific wear, 10 ⁻³ mm ³ /g abrasive					
		15°	30°	45°	60°	75°	90°
ABRASIVE: 27- μ m ALUMINA, NOZZLE ID: 0.58 mm, NOZZLE LENGTH: 1.3 cm							
316 stainless steel (d, 8.070 g/cm ³ , HRB 82.3)	75	62.4	54.1	49.7	41.4	32.5	30.7
	95	67.2	59.0	51.3	45.5	38.1	33.5
	115	92.1	90.4	89.9	80.3	78.5	64.9
	170	240.0	243.0	173.0	147.5	134.8	123.4
440-C stainless steel, annealed (d, 7.780 g/cm ³ , HRC 22.0)	95	42.1	49.9	43.9	37.5	35.2	30.2
	115	88.8	76.4	67.7	51.2	52.2	50.8
	170	179.4	164.3	164.3	132.3	132.3	114.0
440-C stainless steel, hardened (d, 7.780 g/cm ³ , HRC 59.0)	95	57.7	63.2	56.3	53.5	41.9	43.2
	115	101.6	92.7	100.9	93.4	87.2	83.8
	170	197.7	261.6	233.4	161.3	170.9	156.5
HC-250 white cast iron (d, 7.480 g/cm ³ , HRC 63.0)	75	57.7	37.5	39.8	36.6	49.9	35.2
	95	101.6	47.6	46.2	45.8	43.0	43.9
	115	60.9	75.0	69.6	58.6	53.5	61.3
	170	123.6	199.1	167.0	160.6	143.2	175.3
Haynes 6B (d, 8.242 g/cm ³ , HRC 39.0)	75	44.7	46.9	42.6	41.3	33.1	32.3
	95	58.9	67.0	67.0	51.7	44.5	40.9
	115	90.1	88.3	88.3	78.5	76.8	63.5
	170	155.3	185.6	185.6	173.1	143.8	139.0
K-68 cobalt-bonded WC (d, 14.9 g/cm ³ , HRA 92.6)	75	2.9	4.5	8.0	6.9	9.6	10.5
	95	2.0	2.6	5.8	10.3	10.9	12.4
	115	1.4	4.6	10.5	17.3	21.2	17.2
	170	3.7	9.5	27.2	45.4	43.4	43.2
ABRASIVE: 50- μ m ALUMINA, NOZZLE ID: 1.5 mm, NOZZLE LENGTH: 5.3 cm							
316 stainless steel (d, 8.060 g/cm ³ , HRB 82.3)	55	31.2	17.4	15.0	11.9	6.8	5.1
	65	34.1	36.5	28.7	24.2	14.3	24.2
	85	58.0	56.3	43.7	36.2	37.9	25.9
	115	170.4	155.0	148.9	109.3	90.5	86.7
440-C stainless steel, annealed (d, 7.780 g/cm ³ , HRC 22.0)	65	20.4	21.8	19.8	16.7	13.7	11.7
	75	33.8	32.1	28.4	25.1	24.4	23.1
	85	66.6	55.2	47.9	44.5	39.8	29.5
	115	156.6	138.6	142.3	132.2	97.7	78.0
HC-250 white cast iron (d, 7.480 g/cm ³ , HRC 63.0)	55	16.6	19.7	21.0	21.0	17.0	13.9
	65	32.2	36.6	37.0	32.9	27.5	28.5
	85	74.6	75.9	73.9	65.4	58.6	51.9
	115	150.5	172.5	153.6	140.3	129.5	113.9
Haynes 6B (d, 8.242 g/cm ³ , HRC 39.0)	65	18.2	19.6	18.6	18.2	15.5	13.5
	75	38.1	41.5	35.8	30.0	27.7	27.7
	85	57.7	67.5	58.7	51.3	46.9	45.6
	105	83.0	100.2	89.8	75.6	67.2	61.8
	115	130.6	148.2	138.1	120.2	ND	99.9
K-701 cobalt-chromium-bonded WC (d, 14.0 g/cm ³ , HRA 92.0)	65	1.9	2.4	2.3	3.9	3.5	3.0
	75	5.1	6.0	6.2	7.2	6.6	6.6
	85	5.4	11.4	13.2	11.8	12.7	10.1
	105	13.0	18.5	21.6	19.8	21.6	18.6
K-801 nickel-bonded WC (d, 14.8 g/cm ³ , HRA 90.0)	65	1.5	3.2	3.1	4.7	4.2	3.8
	75	1.9	3.9	3.8	7.1	7.2	7.1
	85	3.5	6.0	9.0	11.7	9.9	10.4
	105	5.1	8.7	14.2	15.6	12.0	18.6

ND Not determined.